Planar Polymer Optical Waveguide with Metal-Organic Framework Coating for Carbon Dioxide Sensing

Lei Zheng,* Nils Keppler, Huajun Zhang, Peter Behrens, and Bernhard Roth

An easily fabricated gas sensor based on planar polymer optical waveguides with an integrated zeolite imidazole framework-8 (ZIF-8) thin film is presented for carbon dioxide detection and sensing. The planar optical waveguides are made of polymethylmethacrylate and fabricated by hot embossing, which makes it flexible and cost-efficient. Thin ZIF-8 films are uniformly grown on the waveguides surface through a simple solution method, which is crucial for the envisioned production of metal organic framework-based sensing devices on a large scale. Experimental results show that the produced optical elements exhibit a sensitivity of ≈2.5 µW/5 vol% toward carbon dioxide (CO_2) with very rapid response time (≈6 s) and excellent reversibility of adsorption and desorption of the gas molecules. The demonstrated planar polymer sensing devices provide the potential to develop flexible on-chip gas sensors in an inexpensive and reproducible way.

1. Introduction

The increasing attention paid on environment protection and monitoring makes the selective and sensitive sensing of hazardous and greenhouse gases an important issue in environmental and industrial fields.[1] One of the main greenhouse gases that are largely produced in environment is carbon dioxide (CO_2). In the past decades, many different types of CO_2 sensors have been developed with regard to the operation conditions and application fields. Based on sensing mechanisms, CO_2 sensors can be mainly classified into electrochemical gas

L. Zheng, H. Zhang, B. Roth
Hannover Centre for Optical Technologies
Leibniz University Hannover
30167 Hannover, Germany
E-mail: lei.zheng@hot.uni-hannover.de
L. Zheng, N. Keppler, P. Behrens, B. Roth
Cluster of Excellence PhoenixD (Photonics, Optics, and Engineering-Innovation Across Disciplines)
30167 Hannover, Germany
N. Keppler, P. Behrens
Institute of Inorganic Chemistry
Leibniz University Hannover
30167 Hannover, Germany

The ORCID identification number(s) for the author(s) of this article can be found under https://doi.org/10.1002/admt.202200395.

sensor, optical gas sensor and acoustic gas sensor.[2–4] As a gas sensor works based on the active interaction between the sensing layer and the target gas, the selection and design of sensing material employed in a sensing device plays a significant role in determining the sensing performance. The most commonly used active materials in CO_2 sensing include metal oxide, polymers, carbon materials like carbon nanotubes (CNTs) and graphene, metal-organic frameworks (MOFs) as well as composites of these materials.[5] A general comparison of CO_2 sensors based on different sensing technologies and sensing materials is given in **Table 1**.

With the demand of gas sensors with high sensitivity and selectivity, compact size and low power consumption, MOF-based optical gas sensors, which rely on light–gas interaction within a thin MOF layer, are advantageous due to (i) the properties of minimal drift, high gas specificity to other gases, relevant for the optical gas sensing part and (ii) the high porosity, large surface area and tailor-made pore sizes, relevant for materials part.[8,9] Metal-organic frameworks are porous crystalline materials, which are assembled by the coordination of inorganic building units (IBUs) by organic linker molecules.[10] The pores of MOFs can be refilled with other compounds, therefore they are attractive for applications in various fields, such as gas storage,[11] gas separation,[12] catalysis,[13] and sensing.[14]

The sensing performance of MOF-coated optical sensors can be evaluated by measuring the variations of optical signals (i.e., absorption, transmission, scattering, reflection, etc.) resulting from the refractive index change of structure material due to the filling of the MOF pores with guest gases.[15,16] To date, a variety of MOF-based optical sensors for gas and vapor sensing has been developed, e.g., MOF-coated optical fiber/waveguides and plasmonic nanopatch hold antennas for carbon dioxide (CO_2) selection and sensing,[1,15,17,18] zinc oxide nanorods integrated with MOF for the detection and sensing of hydrogen and benzene,[19] MOF-based Mach–Zehnder interferometer with long period fiber gratings, microring resonators, nanospheres and MOF-embedded gratings for the sensing of volatile organic vapors (i.e., methanol, ethanol, propanol acetone, toluene, benzene, propylene, etc.).[10,20–22] The sensing performance of these optical sensing devices were demonstrated either in the telecommunication wavelength range,[10,17,20] the UV range,[1,21] or the microwave range.[18,19]

In this work, we propose a much simpler and also resource- and cost-efficient gas sensor based on a planar polymer optical

Table 1. General comparisons of CO_2 sensors with different sensing technologies and sensing materials.

(a)

Sensing technologies	Advantages	Disadvantages	Application fields	Ref.
Electrochemical	High sensitivity and selectivity; Possible for online operation; Long lifetime; Low cost.	High power consumption; Cross-sensitive to environment.	Industrial applications; Home/environmental Monitoring.	[3,4]
Optical	High sensitivity and selectivity; Self-reference; Low power consumption; Insensitive to environment.	Affected by ambient interference; Relatively high cost.	Remote air quality monitoring; High-sensitive gas leak detection system.	[2,4]
Acoustic wave	Long lifetime; Battery-free; Avoiding second pollution.	Sensitive to environment variation.	Wireless gas sensor networks.	[2,4]

(b)

Sensing materials	Sensing technologies	Advantages	Disadvantages	Operating temperature	Ref.
Metal oxides (i.e., ZnO, CeO$_2$, etc.)	Electrochemical	Short response time; Low cost; Long-term stability.	Sensitive to environment; High power consumption.	300–700 °C	[4,6]
Polymers (i.e., PEI, PEG, PABA, etc.)	Optical, electrochemical, acoustic wave	High sensitivity; Short response time; Low power consumption; Low cost.	Irreversibility; Relatively poor selectivity.	RT	[4,6]
Carbon materials (i.e., CNTs, graphene, etc.)	Electrochemical	Ultra-high sensitivity; Quick response; Large surface/volume ratio; Low power consumption.	Difficulties in fabrication and repeatability; Toxicity (CNTs).	RT	[4,6]
MOFs (i.e., ZIF, HKUST-1, etc.)	Optical, electrochemical	High sensitivity; Quick response; Large surface area; Simple test procedure.	Long-term instability under humid/acid environment.	RT to 300 °C	[7,8]

Note: ZnO: zinc oxide; CeO$_2$: cerium oxide; PEI: poly(ethylene) imine; PEG: polyethylene glycol; PABA: polyaniline boronic acid; CNTs: carbon nanotubes; ZIF: zeolitic imidazolate frameworks; RT: room temperature.

waveguide with a coated zeolite imidazole framework-8 (ZIF-8) thin film for CO_2 detection and sensing at the near infrared wavelength of 850 nm. ZIF-8 belongs to the group of zeolite-analogue MOFs and possesses much higher thermal and chemical stability than a lot of other MOFs.[23] It has a large surface area of nearly 2000 m^2 g^{-1}, a narrow pore aperture diameter of 3.4 Å, as well as high thermal and chemical stability.[10,23] This enables the efficient adsorption of different gases into the pore area without damage of the framework. With regard to the sorption properties of CO_2 in ZIF-8, a study from McEwan et al. has demonstrated the preferred adsorption of CO_2 over nitrogen (N$_2$) in ZIF-8 at 25 °C and the CO_2 isotherm of ZIF-8 is linear in the range from 0 to 1 bar,[24] which is in good agreement with other publications.[25] Since the zinc ions are shielded by the tetrahedral coordination of the nitrogen atoms of the linker molecules, CO_2 can interact much better with the linker molecules than with the IBUs.[23]

The proposed polymer waveguides can be produced through different techniques, such as direct laser writing by two-photon polymerization,[26] hot embossing replication,[27] imprint lithography,[28] and projection photolithography.[29] Here, we utilized hot embossing, which is a low-cost and rapid approach toward the fabrication of flexible polymer microstructures,

for the replication of proposed optical waveguides made of polymethylmethacrylate (PMMA). A thin ZIF-8 film was grown on top of the produced PMMA waveguides subsequently. Nitrogen and CO_2 were used as the reference gas and the target sensing gas, respectively. An experimental setup was established for the sensing performance characterization. The optical response of the proposed planar waveguide sensor when exposed to pure CO_2 and CO_2 with different concentrations was studied, respectively. The proposed waveguide sensor exhibits a rapid response to CO_2, with the adsorption time of 6 s and desorption time of 16 s. The cycling sensing results show that the proposed waveguide sensor is able to sense CO_2 reliably and reproducibly.

2. Experimental Section

2.1. Materials

In this work, PMMA is employed as the waveguide material. It is a transparent and rigid thermoplastic material, which has a refractive index of ≈1.49 and hence offers high light transmittance. A PMMA sheet (Plexiglas XT 99524, ThyssenKrupp, Germany) was used in the hot embossing process for the

fabrication of polymer waveguides. Zinc nitrate-hexahydrate (98%, Sigma-Aldrich), 2-methylimidazole (99%, Sigma-Aldrich) and methanol (99.5%, Roth) were used without further purification for the growth of MOF film on a structured sample.

2.2. Fabrication of Polymer Waveguides

Hot embossing allows rapid and large-scale replication of structures with dimensions from microscale to centimeter scale. The fabrication procedures are illustrated in detail in **Figure 1**. A structured stamp and a PMMA sheet were first placed onto the upper and lower stages, respectively. They were then heated to 140 °C, which is higher than the glass transition temperature and lower than the melting temperature of PMMA. At this temperature level, the PMMA sheet was in the rubber state and suitable for the subsequent embossing of structure patterns. In the embossing process, the structured stamp was pressed into the PMMA sheet with an embossing force of 4 kN for ≈140 s. A subsequent cooling process followed to cool the stamp and PMMA sheet while maintaining the embossing force. When the temperature reached the demolding temperature (50 °C), the embossing force was released. The stamp and the PMMA sheet could be manually separated. The waveguide sample was then cut into pieces of 20 × 15 mm and cleaned by intensive rinsing with methanol before growing the MOF films on it.

2.3. Growth of MOF Films

ZIF-8 films were grown on samples with the cycled direct growth method.[30] To grow ZIF-8 thin films, stock solutions of 25×10^{-3} M $Zn(NO_3)_2 \cdot 6\,H_2O$ and 50×10^{-3} M 2-methylimidazole in methanol were first prepared, respectively. Afterward, the cleaned substrate was immersed in a mixture of

the two pre-prepared stock solutions (4 mL of each precursor solution, later called synthesis solution) for 30 min at room temperature and rinsed subsequently using pure methanol. The rinsed sample was then incubated into a freshly prepared synthesis solution again to start the next MOF film growth cycle without a drying step in between. This growth process was repeated for three cycles in order to obtain a desired thicker ZIF-8 film (≈300 nm[30]). After the last cycle, the sample was dried in air and was then ready for the sensing performance investigation.
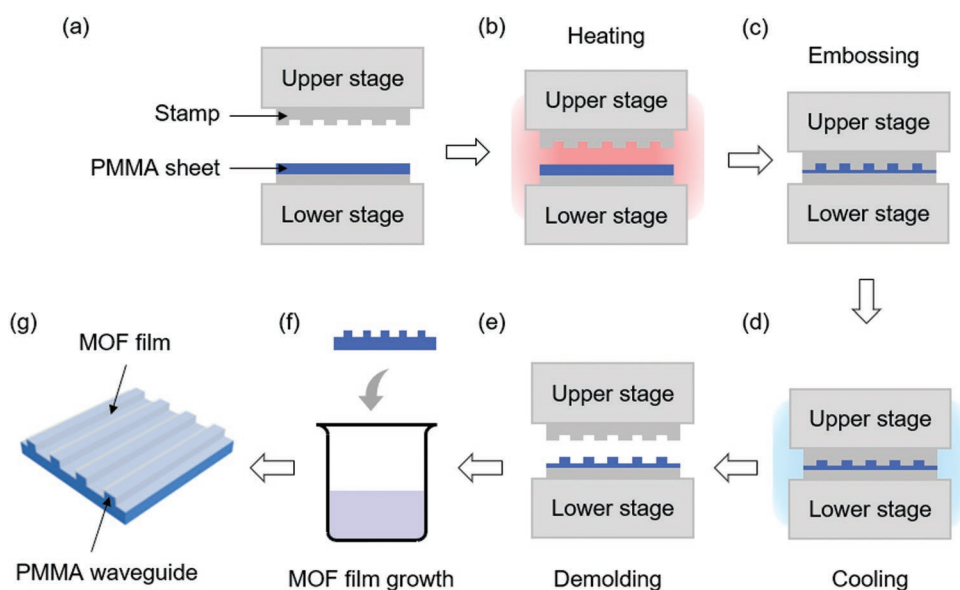
2.4. Characterization Methods

X-ray diffraction (XRD) measurements on ZIF-8 thin films were carried out with an X-ray diffractometer from STOE working in Bragg-Brentano geometry. An Iso-Debyeflex 3003 was used for the generation of X-rays at 40 kV and 30 mA, delivering CuKα_1 radiation. Measurements were performed between 5° and 30° 2θ with a step size of 0.01° 2θ and a measuring time of 20 s per step.
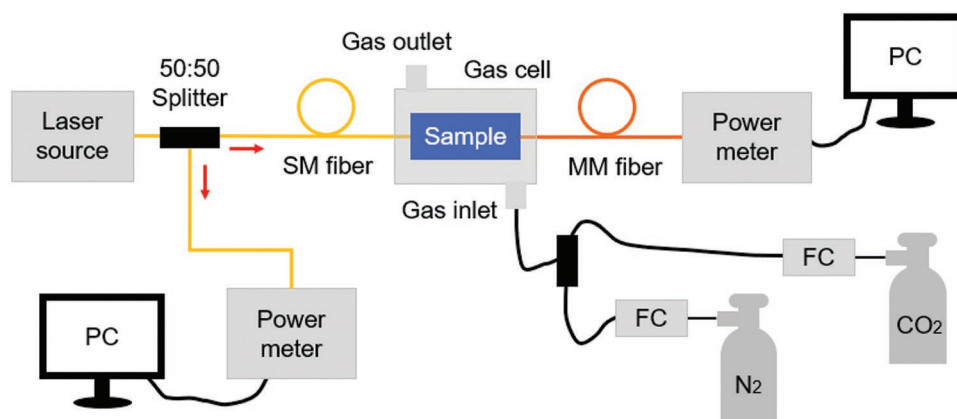
A Sentech SE850 spectroscopic ellipsometer was used to measure the refractive index of ZIF-8. All measurements were performed at angles of 50°, 60°, and 70°. Ellipsometry data were fitted with a Cauchy dispersion model using the software SpectraRay/3. The ellipsometry measurements with variable CO_2 concentrations were performed using mass-flow controllers (El Flow Select, Bronkhorst) for the mixtures of the two gases N_2 and CO_2 in different ratios ranging from 0 to 100 vol% CO_2. These measurements were performed at ambient pressure and temperature. A total flow rate of 0.5 L min^{-1} for both gases was used.

Optical microscopy images of MOF-coated polymer waveguides were acquired using a digital microscope from Keyence (VHX7000) and a 3D optical profiler from Sensofar (S neox).

Scanning electron microscopy (SEM, Joel JSM-6610L V) was also employed to observe prepared samples. For this

Figure 1. Fabrication procedures of MOF-coated waveguides using hot embossing.

**ADVANCED
SCIENCE NEWS**
www.advancedsciencenews.com

**ADVANCED
MATERIALS
TECHNOLOGIES**
www.advmattechnol.de

Figure 2. Schematic illustration of the experimental setup established for the investigation of the gas sensing performance.

characterization, samples were fixed with carbon tape on SEM metal substrate holders. Electrical contact of the thin films was ensured by the use of silver conductive lacquer and by sputtering the samples with a thin layer of gold. SEM images were taken at 10 kV with a working distance of 10 mm.

2.5. Experimental Sensing Setup

A schematic diagram of the established system used for the investigation of gas sensing performance in this study is illustrated in **Figure 2**. A four-channel fiber-coupled laser (Thorlabs Inc.) was used as the light source. The output light was first split by a 1×2 (50:50) coupler. 50% of the light from the laser source was coupled into a power meter (Thorlabs Inc. S151C) as the reference signal. The other 50% was coupled into the MOF-coated polymer waveguide through a single-mode fiber (SM fiber), which was placed inside a self-designed and 3D printed gas cell with a volume of ≈ 38 mL. The gas cell was connected to the N_2 and CO_2 gas cylinders, while allowing for the light incoupling to and outcoupling from the waveguide. The transmitted light was coupled into a multi-mode fiber (MM fiber), which was connected to the power meter. Both the reference and sensing data were collected by computers through USB power and energy meter interfaces (Thorlabs Inc. PM100USB),

respectively. The gas flow was controlled by flow controllers (FC) with a flow range of 0–1 L min^{-1}.

2.6. Statistical Analysis

The normalized transmission data were calculated by taking the output intensity at the stable state when N_2 is purged as the reference gas and $T = 100\%$. Data were presented as mean ± SD. Analysis and measurements of the size of the inhomogeneity sizes were performed using the software ImageJ.

3. Results and Discussion

3.1. Characterization of Materials and Structures

Figure 3a shows the X-ray diffraction (XRD) pattern of a ZIF-8-coated PMMA substrate in comparison to the calculated XRD pattern of ZIF-8.[23] The result confirms the growth of crystalline ZIF-8 on top of the PMMA substrate. All reflections show a good agreement with the literature data. The high background is caused by the amorphous PMMA substrate. A preferred crystal orientation is not visible. Furthermore, the refractive index (RI) of ZIF-8 was measured by ellipsometry. A 200 nm
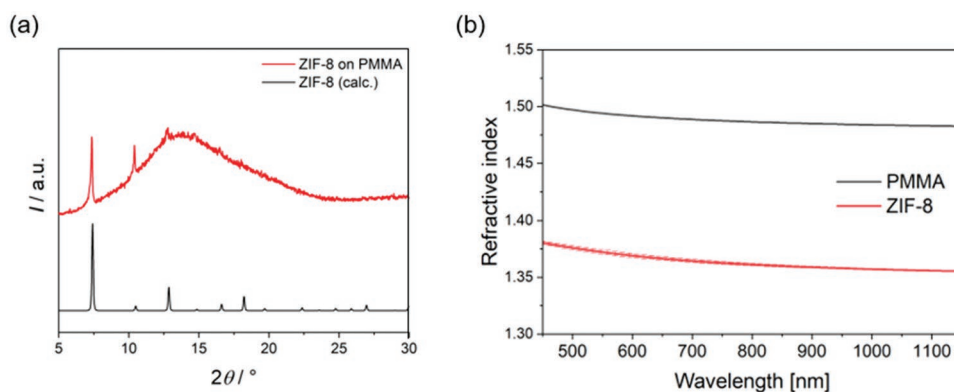
Figure 3. a) XRD measurement of a MOF-coated PMMA substrate. b) The refractive index of PMMA and ZIF-8.
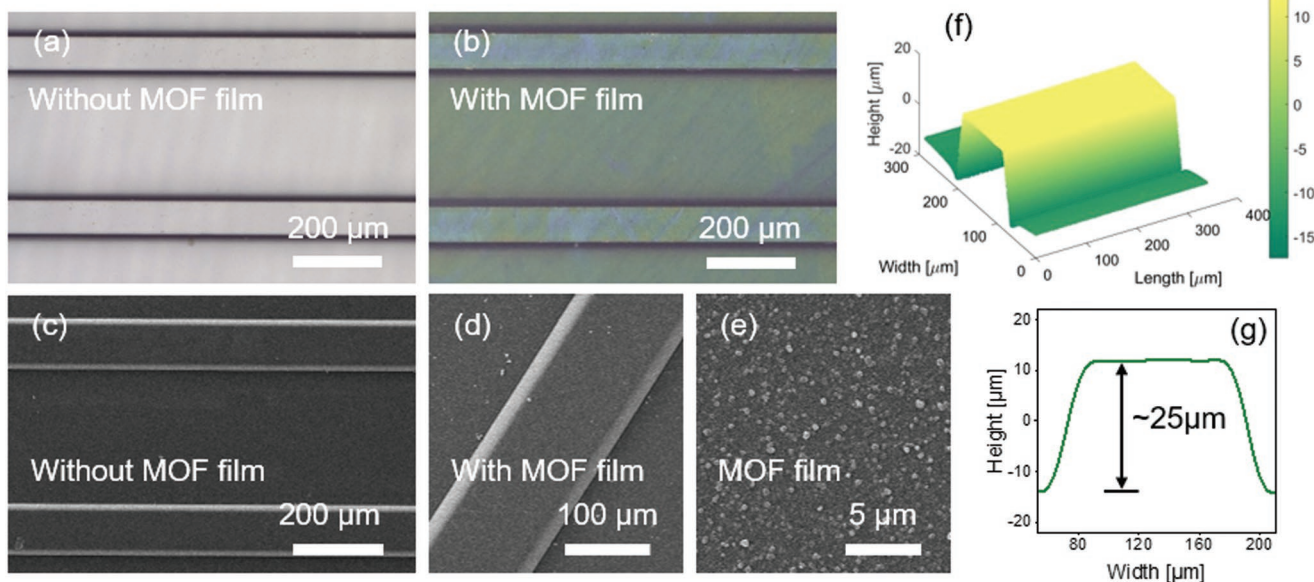
Figure 4. Results from microscopy studies of ZIF-8-coated planar polymer waveguides. Optical microscope images of a) uncoated and b) ZIF-8-coated waveguides. SEM images of an c) uncoated and a d) ZIF-8-coated PMMA waveguide. e) SEM image of a MOF film with higher resolution. f) 3D confocal microscope image of produced PMMA waveguide. g) Height profile of produced PMMA waveguide.

thick film was grown on a silicon wafer for the measurement. The result is shown in Figure 3b. ZIF-8 has a refractive index of 1.36 at the wavelength of 850 nm. As a comparison, the RI of PMMA, which is the material of the waveguide core, is also plotted in the figure. It can be seen that the RI of ZIF-8 is lower than that of the PMMA, which supports the confinement of light modes within the PMMA waveguide core.

The waveguide structures before and after ZIF-8 growth were observed using both optical microscopy (see **Figure 4**a,b) and scanning electron microscopy (SEM, see Figure 4c,d), respectively. The PMMA waveguides shown in Figure 4 have dimensions of ≈100 µm. They exhibit green color after the coating of ZIF-8, as can be seen in Figure 4b. This color is caused by interference effects, while ZIF-8 itself is colorless.[30] ZIF-8 grows in a dense layer on top of the waveguide which is very important for the sensing experiments. Only directly next to the waveguide, a small gap can be seen in Figure S1 (Supporting Information). Further characterization of the coated waveguide surface was performed using AFM and SEM. The AFM topographical images show a densely coated rough surface (see Figure S2, Supporting Information). Analysis of various positions on different waveguides gives an average root-mean-squared roughness of 24.08 ± 3.80 nm. The inhomogeneities on the waveguides surface were determined by measuring a number of inhomogeneity sizes in an SEM image (see Figure S3, Supporting Information) together with subsequent average of those measured data. An average size of 354 ± 96 nm was obtained for these inhomogeneities. The 3D view and profile of the obtained waveguide are shown in Figure 4f,g, demonstrating good structure formation. The measured height of the waveguide from the profile is 25 µm. The dimensions of the waveguide are determined by the master tool used for replication and can be varied over a wide range, from multimode to single mode waveguides.

3.2. Sensing Performance Investigation

The sensing performance of the MOF-coated polymer waveguide was investigated at room temperature and a pressure of 1 bar without any pretreatments such as heating or evacuation under vacuum. The gas cell was first purged with the reference gas with a gas flow rate of 0.2 L min^{-1} for half an hour. After that, the gas was switched from reference gas to CO_2 with a gas flow rate of 0.5 L min^{-1}. The time interval for gas switching, which also indicates the time duration for gas purging, is denoted as Δt. Different concentrations of CO_2 were achieved by controlling the flow rates of N_2 and CO_2. The sum of the flow rates for both gases equals 0.5 L min^{-1}, which is the previously stated flow rate for single gas purging.

Here, sensing performance tests of the proposed device with air as the reference gas were carried out first. The optical responses toward pure CO_2 with different gas changing time interval ($\Delta t = 1$ min and $\Delta t = 30$ s, respectively) and different CO_2 concentrations are shown in Figure S4 (Supporting Information). It can be seen that the optical sensing device exhibits stable and reproducible sensitivity of CO_2 when air is used as the reference gas. These results indicate that the MOF-coated waveguide sensor performs well in the presence of air.

Nevertheless, an inert gas such as nitrogen or argon is usually employed as the reference gas instead of oxygen or air. This is because oxygen might lead to oxidation of the devices. Air consists of different gas compositions including CO_2. This will affect the CO_2 concentration that has been set and makes the experiments not controllable. Additionally, the humidity of air may not be stable when surrounding air is employed as the reference gas. In this work, N_2 is used as the reference gas in the following sensing experiments.

With reference gas N_2, the optical sensing response of a ZIF-8-coated polymer waveguide toward CO_2 was investigated and
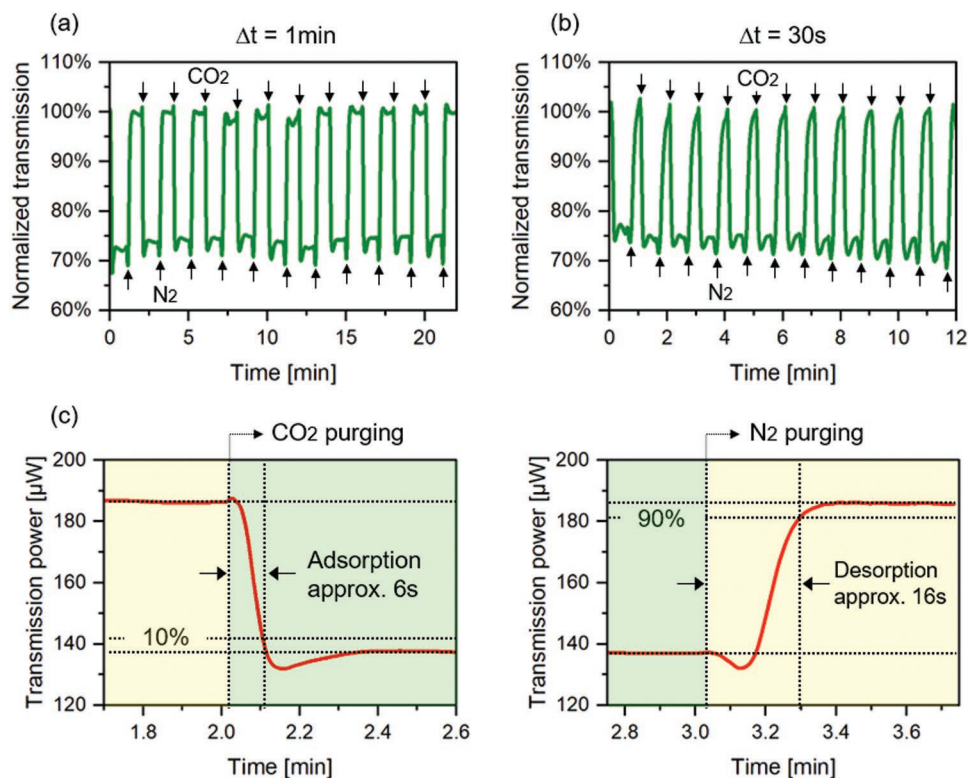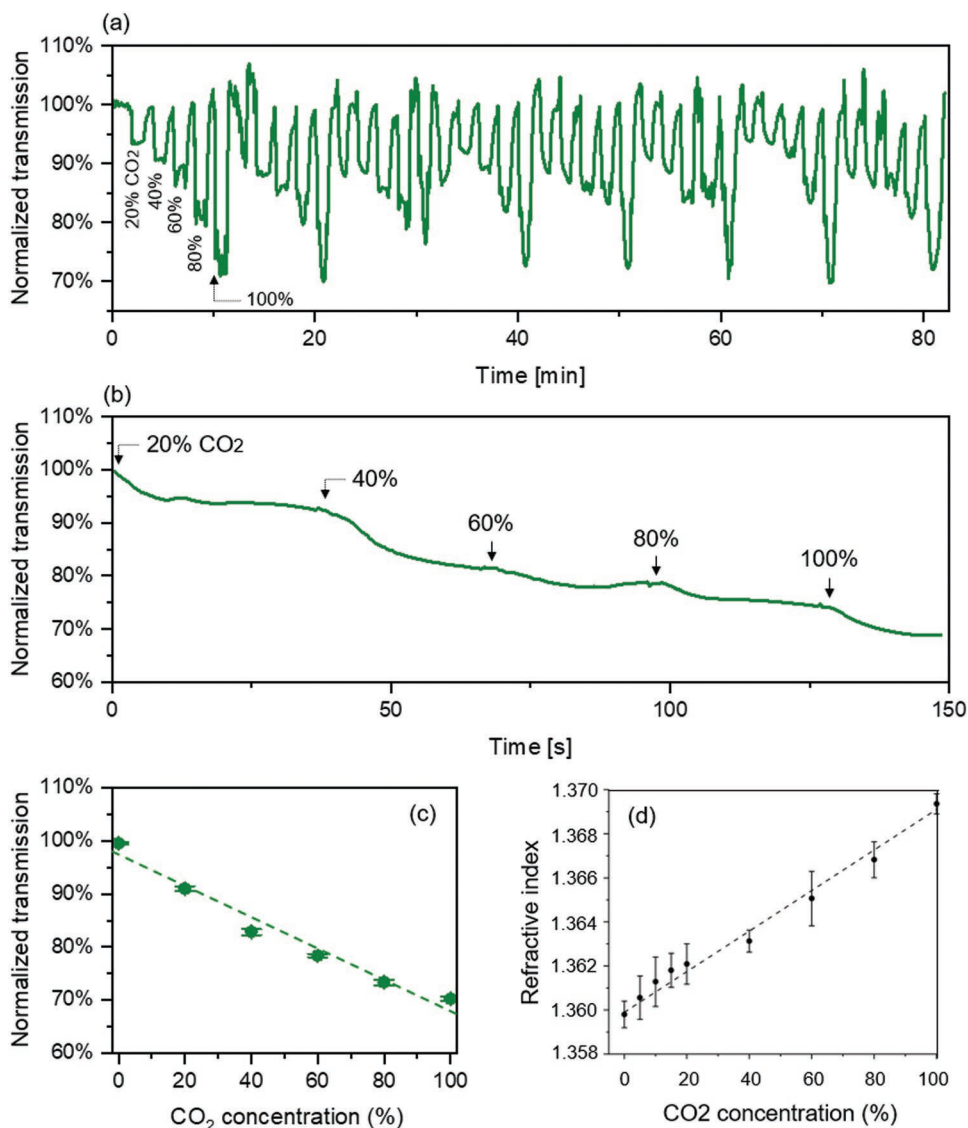
Figure 5. Dynamic optical response of a ZIF-8-coated PMMA waveguide after exposure to CO_2. Response of the MOF-coated waveguide to CO_2 with gas switching time intervals of a) 1 min and b) 30 s. c) Adsorption and desorption time of MOF-coated waveguide sensor.

characterized. Pure N_2 gas was first purged into the gas cell and was then swtiched to CO_2, the stable signal of the former representing the base signal ($T = 100\%$). The optical power out of the MOF-coated waveguide was continuously recorded accordingly. At a steady state, the optical power out of the waveguide is ≈186 µW in the presence of N_2. For a reference, the response of a bare PMMA waveguide toward both gases was investigated, which did not exhibit any signal variation (see Figure S5, Supporting Information). The transmission of optical signals out of the MOF-coated waveguide with a gas switching time interval of $\Delta t = 1$ min was recorded as shown in **Figure 5**a. Multiple repeated cycles were implemented. It can be clearly seen that the transmission signal changed repeatedly and reproducibly with the alternative purging of N_2 and CO_2. When CO_2 was purged into the gas cell, the transmission decreased quickly and stayed in a relatively stable level. The repeated cycling experiments further confirm the sensing functionality and stability of the developed MOF-based polymer waveguides. With the purpose of investigating the optical response of the planar waveguide sensor when exposed to CO_2 in shorter gas switching periods, an additional experiment with $\Delta t = 30$ s was performed. The result is shown in Figure 5b. Also here, the optical signal coming out of the waveguide varies periodically with the alternative purging of N_2 and CO_2. It can also be seen that the high power level when N_2 is purged does not exhibit an obvious steady state due to the short gas switching time. Nevertheless, the multicycling results verify the high reversibility and reproducibility of the sensing performance of proposed planar polymer waveguides.

The response time of a gas sensor to target substances is of great utility for the evaluation of gas diffusion into the MOF sensing layer. The adsorption and desorption time are defined as the time period from the response onset time to 90% of the maximum response in the steady state.[1] As shown in Figure 5c, the MOF-coated PMMA waveguide in this work has the CO_2 adsorption time of ≈6 s and desorption time of ≈16 s, respectively. These results indicate that the diffusion of gases from the surrounding media into the MOF sensing layer is very rapid. The fast adsorption and desorption can be explained by the physical nature of the interaction between ZIF-8 and CO_2. The CO_2 molecules are not chemically bound to the inner MOF surface which allows the guests to leave the pores when the purging of CO_2 from the environment is decreased to a lower concentration or completely stopped. This quick response is a significant advantage for real-world applications in gas sensing. In addition, it can be noticed that the CO_2 desorption time is much longer than the adsorption time. It is well-known from work on polycrystalline membranes that ZIF-8 has a higher selectivity for adsorbing CO_2 in preference over N_2, a result which was recently verified on single-crystal membranes.[31] According to theoretical studies, this is due to the fact that CO_2 molecules exert stronger interactions with the framework than N_2 molecules do.[32]

A further experiment was also carried out to investigate the gas sensing performance of the proposed PMMA waveguide sensor with respect to CO_2 concentration. The transmission obtained on the ZIF-8-coated optical waveguide sensor with different CO_2 concentrations is shown in **Figure 6**a. In this experiment, alternative purging of pure N_2, pure CO_2 and

**ADVANCED
SCIENCE NEWS**

www.advancedsciencenews.com

**ADVANCED
MATERIALS
TECHNOLOGIES**

www.advmattechnol.de

Figure 6. a) Dynamic response of the ZIF-8-coated waveguide sensor with respect to different CO_2 concentrations under the alternative purging of pure N_2 and a gas mixture of N_2 and CO_2. b) Dynamic response of the ZIF-8-coated waveguide sensor with respect to different CO_2 concentrations without the purging of pure N_2 in between the changing of CO_2 concentration. c) The transmission as a function of CO_2 concentration. d) The measured refractive index of ZIF-8 film at different CO_2 concentrations.

the mixtures of N_2 and CO_2 with different concentrations was chosen. It can be seen from the eight cycling results that lower transmission is obtained with higher CO_2 concentration in almost all cycles. This indicates higher signal changes of the ZIF-8-coated planar polymer waveguide sensor with the increase of CO_2 concentration and demonstrates the reversibility of this ZIF-8-coated polymer waveguide sensor. Sensing performance of the same waveguide sensor in the case of direct reduction of CO_2 concentration without the purging of N_2 to recover the transmission signal was investigated as well (see Figure 6b). The transmission values were recorded with CO_2 concentrations of 0, 20, 40, 60, 80, and 100 vol%. These reveal a steady decrease with the increase of CO_2 concentration. A linear fit of the transmission at each CO_2 concentration was also carried out (see Figure 6c). This result indicates the

quantifiable relations between the transmission and CO_2 concentration. Within this CO_2 concentration range, the sensing device has a sensitivity of ≈2.5 µW/5 vol%, which is estimated based on the linear fit. A set of corresponding cycling experiments was also carried out with the result shown in Figure S6 (Supporting Information).

The higher decrease of the transmission with increasing CO_2 concentrations can be explained by changes of the MOFs refractive index resulting from the varying adsorption of CO_2 molecules from the environment at different CO_2 concentrations (see Figure 6d). The refractive index of ZIF-8 increases approximately linearly with increasing CO_2 concentration. This is also the case for the transmission that decreases with increasing concentration. The evanescent field effect[33] gives a good explanation for this: light propagates in the waveguide

core material, which has a higher refractive index than the surrounding material, based on internal reflection at the interface between the waveguide (core, PMMA) and the coated layer (ZIF-8). A higher refractive index difference between the core material and coating material leads to stronger reflection at the interface, thus, a higher output signal from the waveguide results. On the other side, a lower refractive index difference between the core and coating materials results in a higher intensity loss. When CO_2 is purged into the MOF sensing layer, the refractive index increase of the MOF lowers the refractive index difference. As a result, a decrease of the transmission output signal of the sensing device was measured. The experimental result shows that there is only tiny transmission change at low CO_2 concentrations (see Figure S7, Supporting Information). This can be explained by the small refractive index increase of ZIF-8 due to CO_2 adsorption at low CO_2 concentrations. The result in Figure S7 (Supporting Information) reveals a limit of detection (LOD) down to 5 vol%, as the transmission variation percentage from the neighboring higher (7.5 vol%, transmission variation ≈1%) or lower (2.5 vol%, transmission variation ≈0.5 vol%)) concentrations to this concentration is detectable.

4. Conclusion

In this work, we demonstrate a planar polymer waveguide sensor coated with ZIF-8 thin films for CO_2 sensing. A low-cost and efficient hot embossing technique was introduced for the fabrication of the proposed waveguide structure together with an easy-to-implement technique for the realization of the MOF film. Multimode waveguide structures were employed for the investigations. The waveguide sensor shows sensitive optical response to pure CO_2 as well as CO_2 with different concentrations. A sensitivity of ≈2.5 µW/5 vol% and LOD down to 5 vol% were obtained. The sensing device also exhibits rapid response to the target sensing gas, with adsorption time of 6 s and desorption time of 16 s, respectively. Sets of cycling experiments demonstrate the reversibility and reproducibility of the sensing performance of the proposed planar polymer waveguide sensor. This proof-of-concept study enables a more flexible fabrication of polymer waveguides, simplifies the introduction of MOF-based optical devices and thus opens up new application potentials of this material combination for selective gas detection and sensing. The achievable sensitivity of the approach and the cross-sensitivities to other gases and environmental parameters will be studied in further steps.

Supporting Information

Supporting Information is available from the Wiley Online Library or from the author.

Acknowledgements

Conflict of Interest

The authors declare no conflict of interest.

Data Availability Statement

The data that support the findings of this study are available from the corresponding author upon reasonable request.

Keywords

[1] K.-J. Kim, P. Lu, J. T. Culp, P. R. Ohodnicki, *ACS Sens.* **2018**, *3*, 386.
[2] Z. Yunusa, M. N. Hamidon, A. Kaiser, Z. Awang, *Sens. Transducers* **2014**, *168*, 61.
[3] S. Neethirajan, D. S. Jayas, S. Sadistap, *Food Bioprocess Technol.* **2009**, *2*, 115.
[4] X. Liu, S. Cheng, H. Liu, S. Hu, D. Zhang, H. Ning, *Sensors* **2012**, *12*, 9635.
[5] C. Love, H. Nazemi, E. El-Masri, K. Ambrose, M. S. Freund, A. Emadi, *Sensors* **2021**, *21*, 3423.
[6] A. Molina, V. Escobar-Barrios, J. Oliva, *Synth. Met.* **2020**, *270*, 116602.
[7] X. Fang, B. Zong, S. Mao, *Nano-Micro Lett.* **2018**, *10*, 64.
[8] H. Yuan, N. Li, W. Fan, H. Cai, D. Zhao, *Adv. Sci.* **2022**, *9*, 2104374.
[9] J. Hodgkinson, R. P. Tatam, *Meas. Sci. Technol.* **2013**, *24*, 012004.
[10] J. Wu, W. Zhang, Y. Wang, B. Li, T. Hao, Y. Zheng, L. Jiang, K. Chen, K. S. Chiang, *Nanoscale* **2020**, *12*, 9991.
[11] a) D. Gygi, E. D. Bloch, J. A. Mason, M. R. Hudson, M. I. Gonzalez, R. L. Siegelman, T. A. Darwish, W. L. Queen, C. M. Brown, J. R. Long, *Chem. Mater.* **2016**, *28*, 1128; b) Y. Ji, L. Ding, Y. Cheng, H. Zhou, S. Yang, F. Li, Y. Li, *J. Phys. Chem. C* **2017**, *121*, 24104; c) X. Yang, Q. Xu, *Cryst. Growth Des.* **2017**, *17*, 1450.
[12] a) U. Böhme, B. Barth, C. Paula, A. Kuhnt, W. Schwieger, A. Mundstock, J. Caro, M. Hartmann, *Langmuir* **2013**, *29*, 8592; b) L. Fan, Z. Kang, Y. Shen, S. Wang, H. Zhao, H. Sun, X. Hu, H. Sun, R. Wang, D. Sun, *Cryst. Growth Des.* **2018**, *18*, 4365; c) A. Knebel, B. Geppert, K. Volgmann, D. I. Kolokolov, A. G. Stepanov, J. Twiefel, P. Heitjans, D. Volkmer, J. Caro, *Science* **2017**, *358*, 347.
[13] a) H. Beyzavi, N. A. Vermeulen, A. J. Howarth, S. Tussupbayev, A. B. League, N. M. Schweitzer, J. R. Gallagher, A. E. Platero-Prats, N. Hafezi, A. A. Sarjeant, J. T. Miller, K. W. Chapman, J. Fraser Stoddart, C. J. Cramer, J. T. Hupp, O. K. Farha, *J. Am. Chem. Soc.* **2015**, *137*, 13624; b) L. Mitchell, P. Williamson, B. Ehrlichová, A. E. Anderson, V. R. Seymour, S. E. Ashbrook, N. Acerbi, L. M. Daniels, R. I. Walton, M. L. Clarke, P. A. Wright, *Chemistry* **2014**, *20*, 17185.
[14] a) Z. Hu, C. Tao, H. Liu, X. Zou, H. Zhu, J. Wang, *J. Mater. Chem. A* **2014**, *2*, 14222; b) J.-W. Ye, H.-L. Zhou, S.-Y. Liu, X.-N. Cheng, R.-B. Lin, X.-L. Qi, J.-P. Zhang, X.-M. Chen, *Chem. Mater.* **2015**, *27*, 8255; c) J. F. Olorunyomi, S. T. Geh, R. A. Caruso, C. M. Doherty, *Mater. Horiz.* **2021**, *8*, 2387; d) M.-S. Yao, J.-W. Xiu, Q.-Q. Huang, W.-H. Li, W.-W. Wu, A.-Q. Wu, L.-A. Cao, W.-H. Deng, G.-E. Wang, G. Xu, *Angew. Chem., Int. Ed.* **2019**, *58*, 14915.

**ADVANCED
SCIENCE NEWS**

www.advancedsciencenews.com

**ADVANCED
MATERIALS
TECHNOLOGIES**

www.advmattechnol.de

[15] C. Zhu, R. E. Gerald, J. Huang, *IEEE Sens. J.* **2021**, *21*, 19647.

[16] G. Lu, J. T. Hupp, *J. Am. Chem. Soc.* **2010**, *132*, 7832.

[17] X. Chong, K.-J. Kim, P. R. Ohodnicki, E. Li, C.-H. Chang, A. X. Wang, *IEEE Sens. J.* **2015**, *15*, 5327.

[18] X. Chong, Y. Zhang, E. Li, K.-J. Kim, P. R. Ohodnicki, C.-H. Chang, A. X. Wang, *ACS Sens.* **2018**, *3*, 230.

[19] A. I. Khudiar, A. K. Elttayef, M. K. Khalaf, A. M. Oufi, *Mater. Res. Express* **2019**, *6*, 126450.

[20] J. Tao, X. Wang, T. Sun, H. Cai, Y. Wang, T. Lin, D. Fu, L. L. Y. Ting, Y. Gu, D. Zhao, *Sci. Rep.* **2017**, *7*, 41640.

[21] X. Huang, S. Yan, D. Deng, L. Zhang, R. Liu, Y. Lv, *ACS Appl. Mater. Interfaces* **2021**, *13*, 3471.

[22] O. Dalstein, D. R. Ceratti, C. Boissière, D. Grosso, A. Cattoni, M. Faustini, *Adv. Funct. Mater.* **2016**, *26*, 81.

[23] K. S. Park, Z. Ni, A. P. Côté, J. Y. Choi, R. Huang, F. J. Uribe-Romo, H. K. Chae, M. O'Keeffe, O. M. Yaghi, *Proc. Natl. Acad. Sci. USA* **2006**, *103*, 10186.

[24] J. McEwen, J.-D. Hayman, A. Ozgur Yazaydin, *Chem. Phys.* **2013**, *412*, 72.

[25] a) Z. Xiang, X. Peng, X. Cheng, X. Li, D. Cao, *J. Phys. Chem. C* **2011**, *115*, 19864; b) Z. Zhang, S. Xian, Q. Xia, H. Wang, Z. Li, J. Li, *AIChE J.* **2013**, *59*, 2195.

[26] L. Zheng, K. Kurselis, A. El-Tamer, U. Hinze, C. Reinhardt, L. Overmeyer, B. Chichkov, *Nanoscale Res. Lett.* **2019**, *14*, 134.

[27] M. Rezem, A. Günther, M. Rahlves, B. Roth, E. Reithmeier, *Proc. Technol.* **2014**, *15*, 514.

[28] F. Hua, Y. Sun, A. Gaur, M. A. Meitl, L. Bilhaut, L. Rotkina, J. Wang, P. Geil, M. Shim, J. A. Rogers, A. Shim, *Nano Lett.* **2004**, *4*, 2467.

[29] L. Zheng, U. Zywietz, T. Birr, M. Duderstadt, L. Overmeyer, B. Roth, C. Reinhardt, *Microsyst. Nanoeng.* **2021**, *7*, 64.

[30] N. C. Keppler, K. D. J. Hindricks, P. Behrens, *RSC Adv.* **2022**, *12*, 5807.

[31] C. Chen, A. Ozcan, A. O. Yazaydin, B. P. Ladewig, *J. Membr. Sci.* **2019**, *575*, 209.

[32] T. Chokbunpiam, S. Fritzsche, C. Chmelik, J. Caro, W. Janke, S. Hannongbua, *J. Phys. Chem. C* **2016**, *120*, 23458.

[33] R. Orghici, U. Willer, M. Gierszewska, S. R. Waldvogel, W. Schade, *Appl. Phys. B* **2008**, *90*, 355.